Theor Chem Acc (2002) 107:336–342
DOI 10.1007/s00214-002-0338-x

Theoretical
Chemistry Accounts

Regular article

Density functional computation of ^{55}Mn NMR parameters

Michael Bühl

Max-Planck-Institut für Kohlenforschung, Kaiser-Wilhelm-Platz 1, 45470 Mülheim an der Ruhr, Germany
e-mail: buehl@mpi-muelheim.mpg.de

Received: 17 January 2002 / Accepted: 13 March 2002 / Published online: 3 June 2002

Abstract. Gradient-corrected (GGA) and hybrid variants of density functional theory are used to compute geometries and ^{55}Mn chemical shifts of MnO_4^-, $Mn(CO)_6^+$, $Mn_2(CO)_{10}$, $Mn(CO)_5X$ [$X = H$, Cl, C(O)Me], $Mn(CO)_5^-$, $Mn(NO)_3(CO)$, and $Mn(C_5H_5)L_x$ [$L_x = (CO)_3$, C_6H_6, C_7H_8]. For this set of compounds, substituent effects on $\delta(^{55}Mn)$ are significantly underestimated with the pure GGA functional BPW91 and are well described with hybrid functionals such as mPW1PW91 and, in particular, B3LYP. The computed data provide evidence for solvent and counterion effects on $\delta(^{55}Mn)$ of MnO_4^- and $Mn(CO)_6^+$, respectively. The latter, in the presence of Cl^-, may be described as highly fluxional $Mn(CO)_5C(O)Cl$. Electric field gradients computed with the B3LYP functional can be used for a qualitative rationalization of observed trends in ^{55}Mn NMR line widths. Electronic supplementary material to this paper can be obtained by using the Springer LINK server located at http://dx.doi.org/10.1007/s00214-002-0338-x

Key words: ^{55}Mn NMR – Density functional calculations – Chemical shift computations – Electric field gradients – NMR line widths

1 Introduction

Approximate quantum chemical methods need performance tests for their validation. This is particularly true for the modern tools of density functional theory (DFT), as the extent of the success or failure of a given density functional is hard to estimate beforehand. Experience regarding the performance and reliability of the various flavors of DFT is being accumulated rapidly [1]. The present-day gradient-corrected (GGA) or hybrid functionals are robust enough that, for instance, "computational transition-metal chemistry today is almost synonymous with DFT for medium-sized molecules" [2]. Structures and energetics, as well as vibrational and NMR spectroscopical properties of transition-metal complexes can be computed and predicted with reasonable accuracy [1]. Transition-metal NMR chemical shifts have proven to be quite sensitive to the specific density functional employed, and are thus a particularly stringent test for the quality of the latter [3]. For the majority of nuclei investigated so far, the popular B3LYP hybrid functional has performed noticeably better than "pure" GGA functionals such as BPW91 [4–7]. The sole exceptions encountered to date are ^{95}Mo chemical shifts, where the opposite has been found [8]. It has thus been concluded that for each new nucleus, the density functionals have to be reassessed carefully. In the present work, such performance tests are reported for ^{55}Mn chemical shifts. Individual theoretical $\delta(^{55}Mn)$ values have been communicated previously [9], but no systematic survey covering the total chemical shift range has appeared yet.

As with practically every NMR-active transition-metal nucleus, ^{55}Mn has a trait that diminishes its attractivity for NMR spectroscopy, in this case a large quadrupole moment [10]. Despite the resulting propensity for line broadening, sometimes preventing detection of the signal altogether, there is a sizeable amount of $\delta(^{55}Mn)$ data [10–12]. Furthermore, ongoing developments in NMR methodology and technology facilitate observation of nuclei in compounds hitherto believed to pose unsurmountable problems [13]. Since transition-metal NMR presents itself more than ever as a sensitive probe for structure and reactivity of organometallic and coordination compounds [14], reliable first-principles computations of the salient NMR parameters are becoming more and more important. The systematic study of theoretical ^{55}Mn chemical shifts presented here is intended to expand the list of nuclei for which this is already possible.

Correspondence to: M. Bühl

Electronic supplementary material to this paper can be obtained by using the Springer LINK server located at http://dx.doi.org/10.1007/s00214-002-0338-x

As already mentioned, the line widths of the ^{55}Mn resonances can be an important issue. For quadrupolar nuclei, the line widths can depend on the degree of anisotropy of the electron distribution about the metal nucleus. A highly unsymmetric electron distribution gives rise to a large electric field gradient (EFG) and, by virtue of an efficient quadrupolar relaxation mechanism, to a broadening of the signal. Line widths exceeding 10 kHz are not uncommon [10–12] and, as with many other quadrupolar transition-metal nuclei [15], the resonances may even become too broad to be detected. Computed EFGs have been used before to rationalize observed trends in ^{91}Zr, ^{71}Ga, and ^{99}Ru line widths [6, 16]. A corresponding study is now included for manganese complexes.

2 Computational methods

The methods and the basis sets correspond to those used in previous studies of first-row transition-metal complexes [4]. The geometries were fully optimized in the given symmetry at the BP86/AE1 level, i.e., by employing the exchange and correlation functionals of Becke [17] and Perdew [18], respectively, together with a fine integration grid (75 radial shells with 302 angular points per shell), the augmented Wachters basis for Mn [19] (contraction scheme 62111111/3311111/3111), and standard 6-31G* basis set [20] for all other elements. All structures (except **10**) were characterized as minima by the absence of imaginary harmonic vibrational frequencies. The geometries are given as supporting material in the form of Cartesian coordinates.

Magnetic shieldings, σ, were evaluated for the BP86/AE1 geometries using a recent implementation of the gauge-including atomic orbitals (GIAO)–DFT method [21], involving the functional combinations according to Becke [17] and Perdew and Wang [22] (denoted BPW91), mPW1PW91 [23] or Becke (hybrid) [24] and Lee, Yang, and Parr [25] (denoted B3LYP), together with basis II′, i.e., the same Wachters basis on Mn and the recommended IGLO basis II [26] on all other atoms except H, for which a double-zeta basis was used ([2s] contraction [26]); for the hydride **4**, basis II was also used on hydrogen ([3s1p] contraction), and the 6-31G** basis was used on H during geometry optimization. The absolute shielding of the reference, saturated aqueous $KMnO_4$, was evaluated from the correlation of computed σ versus experimental δ values (taken from Refs. [10–12]) for the set of compounds in this study (cf. the procedure for theoretical ^{103}Rh and ^{99}Ru chemical shifts [4, 6]), resulting in σ(standard) values of −3,109, −4,848, and −4,506 ppm at the GIAO–BPW91, GIAO–mPW1PW91, and GIAO–B3LYP levels, respectively.

EFGs were computed at the B3LYP/II′ level employing the BP86/AE1 geometries. The largest component of the EFG tensor, q_{zz}, is given (reported in atomic units, 1 au = 9.717365×10^{21} Vm^{-2} for conversion into eq values). All the computations employed the Gaussian 98W program [27].

3 Results and discussion

3.1 Geometries

The test set comprised MnO_4^- (**1**) and the organometallic species **2**–**11** (Fig. 1). The important optimized geometrical parameters are collected in Table 1, together with corresponding data observed in the solid state [28–34] or in the gas phase [35, 36], where available. In general, the theoretical data compare favorably to the experimental values, with bond lengths typically

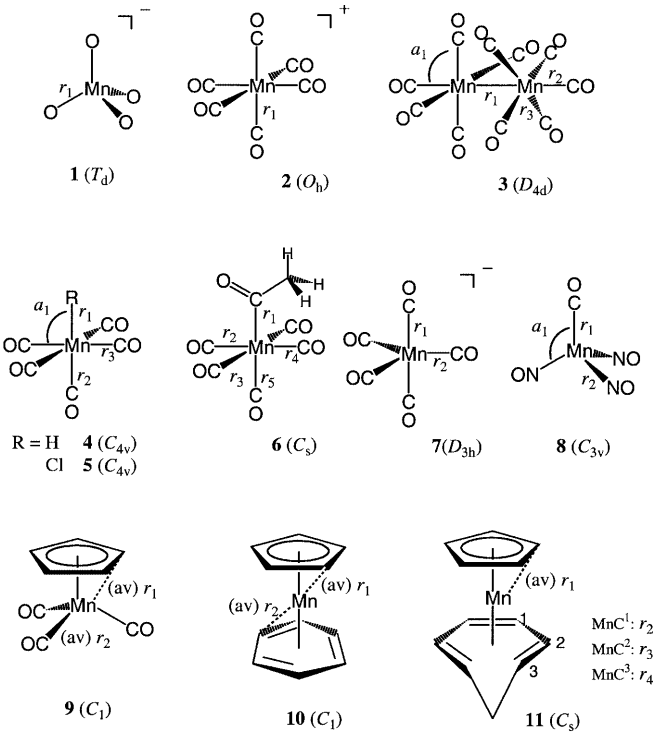

Fig. 1. Manganese complexes **1**–**11** of this study. Computed and experimental data for the indicated key geometrical parameters are given in Table 1

agreeing to a few picometers. The optimized bond distances tend to be overestimated, in particular if compared to those determined in the solid state, but are mostly within experimental error (taken as 3σ).

The cyclopentadienyl (Cp) compounds **9**–**11** are characterized by low rotational barriers of the Cp group with respect to the other ligands (all below 0.5 kcal/mol at the BP86/AE1 + ZPE level). The orientations shown in Fig. 1 correspond to minima at the BP86/AE1 level, except for **10**, where a small imaginary frequency, $14i$ cm^{-1}, remains even when the optimization is carried out in C_1 symmetry. Very likely, this is an artifact due to a too small grid in the numerical integration. Reoptimization using a larger grid would probably rectify this problem; however, since only minor changes in the geometrical parameters (and, thus, in the resulting magnetic shieldings) are to be expected, such a reoptimization was not pursued.

3.2 Chemical shifts

The ^{55}Mn chemical shifts are referenced to a saturated aqueous solution of $KMnO_4$ [10]. When an isolated MnO_4^- ion (**1**) was used to model this standard, i.e., when the computed magnetic shieldings for **2**–**11** were referenced directly relative to that of **1**, the resulting δ values showed systematic deviations towards lower frequency (higher field) compared to experiment. Apparently, the magnetic shielding of **1** is affected more strongly by the solvent water than those of the organometallic species by the aprotic solvents. Solvent

effects on chemical shifts can be modeled computationally, for instance, using molecular-dynamics-based approaches [37], but this is beyond the scope of this work. Instead, the reference shielding value was evaluated from σ_{calc} versus δ_{expt} correlations as detailed in Section 2. The resulting ^{55}Mn chemical shifts, computed at the GIAO–BPW91, GIAO–mPW1PW91, and GIAO–B3LYP levels are summarized in Table 2 (note that the resulting δ values for **1** differ substantially from zero).

The calculated δ values are plotted versus the experimental data in Fig. 2. The best agreement with experiment is obtained at the GIAO–B3LYP level, as evidenced by the near-ideal slope of 0.99 for the δ_{calc} versus δ_{exp} linear regression. Nearly the same degree of agreement with experiment is obtained with the mPW1PW91 data, even though the corresponding slope is somewhat larger, 1.09. In contrast, the pure GGA functional BPW91 affords a slope much smaller than unity, 0.72. Thus, substituent effects on $\delta(^{55}\text{Mn})$ are substantially underestimated with this functional, which leads to large absolute deviations from experiment, on average $\Delta\delta = 484$ (Table 2). Despite the near-ideal slopes obtained with the mPW1PW91 and, in particular, the B3LYP functionals, a noticeable scatter is apparent in the corresponding δ_{calc} versus δ_{exp} plots (Fig. 2). The mean absolute deviations from experiment for the latter two functionals is $\Delta\delta = 242$ and 215, respectively (Table 2). The latter error corresponds to roughly 5% of the total chemical shift range covered, $\Delta\delta \approx 4000$, and is slightly larger than the errors obtained for the other transition-metal nuclei investigated so far (between about 2% for ^{99}Ru and 4% for ^{57}Fe) [4, 6]). Theoretical data of this accuracy may still be useful, for instance, for the interpretation of large differences in $\delta(^{55}\text{Mn})$ values

Table 1. BP86/AE1 optimized geometrical parameters for Mn complexes **1**–**10** (angstroms and degrees, see Fig. 1 for definition of parameters); in *italics*: experimental values from X-ray crystallography, except where otherwise noted. In cases where the symmetry in the crystal is lower than that indicated in Fig. 1, correspondingly averaged values are given (in *parentheses*: estimated standard deviations)

Molecule	r_1	r_2	r_3	r_4	a_1	Ref.
MnO_4^- (**1**)	1.625					
	1.629 ± 0.005					[28]
$Mn(CO)_6^+$ (**2**)	1.897					
$Mn_2(CO)_{10}$ (**3**)	2.965	1.812	1.857		93.8	
	2.977(11)	*1.803(16)*	*1.873(5)*		*93.4(5)*	[35][a]
	2.904(1)	*1.820(2)*	*1.853(1)*		*93.9(1)*	[29]
$Mn(CO)_5H$ (**4**)	1.578	1.851	1.851		96.8	
	1.50(7)	*1.860(4)*	*1.860(4)*		*96.4(10)*	[36][a]
	1.601(16)	*1.822(12)*	*1.853(13)*		*97.1(5)*	[30][b]
$Mn(CO)_5Cl$ (**5**)	2.399	1.818	1.872		94.3	
	2.367(4)	*1.807(9)*	*1.893(6)*		*91.8(3)*	[31]
$Mn(CO)_5COMe$ (**6**)	2.203	1.865	1.853	1.853	r_5: 1.846	
$Mn(CO)_5^-$ (**7**)	1.833	1.814				
	1.820(11)	*1.798(12)*				[32]
$Mn(NO)_3(CO)$ (**8**)	1.861	1.699			105.2	
$Mn(Cp)(CO)_3$ (**9**)	2.168	1.795				
	2.138(3)	*1.793(3)*				[33]
$Mn(Cp)(C_6H_6)$ (**10**)	2.111	2.098				
	2.124(5)	*2.106(5)*				[34][c]
$Mn(Cp)(C_7H_8)$ (**11**)	2.121	2.116	2.102	2.168		

[a] Gas-phase electron diffraction
[b] Neutron diffraction
[c] $Mn(Cp)(C_6H_5Ph)$ derivative

Table 2. Theoretical ^{55}Mn chemical shifts, computed at the GIAO–DFT level with BP86/AE1 geometries and basis II′, together with experimental data

Molecule	GIAO–BPW91	GIAO–mPW1PW91	GIAO–B3LYP	Expt.[a]
MnO_4^- (**1**)	530	260	325	0
$Mn(CO)_6^+$ (**2**)	−1,375	−2,051	−1,848	−1,445
$Mn_2(CO)_{10}$ (**3**)	−1,667	−2,520	−2,282	−2,325
$Mn(CO)_5H$ (**4**)	−1,948	−2,914	−2,788	−2,578
$Mn(CO)_5Cl$ (**5**)	−1,064	−1,574	−1,424	−1,004
$Mn(CO)_5COMe$ (**6**)	−1,329	−2,121	−1,904	−1,851
$Mn(CO)_5^-$ (**7**)	−1,780	−2,743	−2,487	−2,780
$Mn(NO)_3(CO)$ (**8**)	−522	−962	−835	−1,171
$Mn(Cp)(CO)_3$ (**9**)	−1,571	−2,193	−2,009	−2,225
$Mn(Cp)(C_6H_6)$ (**10**)	−306	−180	−231	−180
$Mn(Cp)(C_7H_8)$ (**11**)	646	1,224	1,065	1,077
Slope[b]	0.72	1.09	0.99	
Mean absolute deviation[c]	484	242	215	

[a] Experimental $\delta(^{55}\text{Mn})$ data from Refs. [10, 11, 12]
[b] Slope of the δ_{calc} versus δ_{exp} linear regression
[c] Mean absolute deviation of theoretical versus experimental data

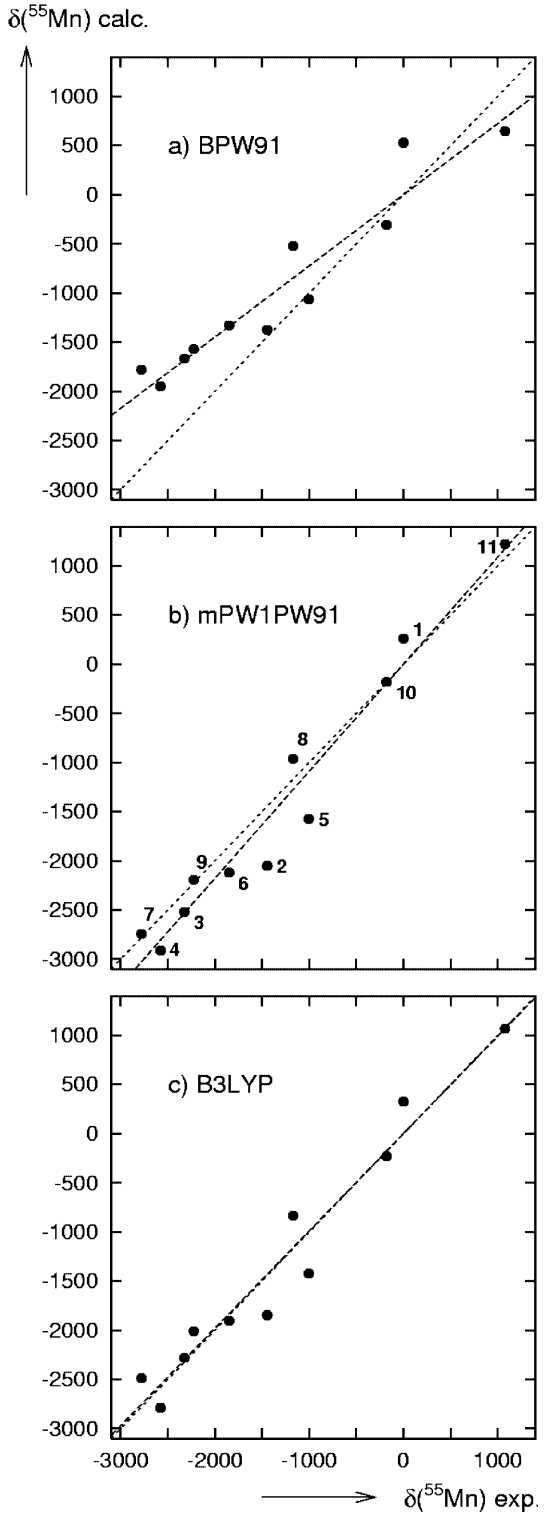

Fig. 2a–c. Plot of computed (basis II′ for BP86/AE1 optimized geometries) versus experimental ^{55}Mn chemical shifts. **a** GIAO–BPW91, **b** GIAO–mPW1PW91, **c** GIAO–B3LYP level. Linear regression lines (*dashed*) and ideal lines with slope 1 (*dotted*) are included

of related compounds (see later). Occasional larger deviations from experiment notwithstanding, the results presented here strongly argue in favor of inclusion of Hartree–Fock exchange in ^{55}Mn chemical shift calculations. Thus, Mn joins the group of transition-metal nuclei [4–7] for which hybrid functionals such as B3LYP outperform pure GGA functionals. In that respect, ^{95}Mo remains the only exception encountered so far [8].

Complexes **1** and **2** have already been the subject of DFT performance tests for $\delta(^{55}\mathrm{Mn})$ [9]. Large deviations for $\delta(^{55}\mathrm{Mn})$ of **2** relative to **1** from experiment have been noted for both GGA and hybrid functionals, of the order of $\Delta\delta \approx -700$ and -740, respectively (employing an optimized geometry for **2**). Similar deviations are encountered with the methods employed in the present study when the shielding differences between **1** and **2** are considered. As already mentioned, part of the errors stem from apparent problems with the description of the standard, **1**. With the shift data given in Table 2 (relative to the fitted standard), corresponding deviations from experiment of $\Delta\delta \approx 70$ and -400 are obtained with BPW91 and B3LYP, respectively. It follows from the analysis given here that the good performance of the former, nonhybrid GGA in this case is largely fortuitous. Performance tests for chemical shift computations should employ larger sets of compounds.

Part of the residual error of the B3LYP value for **2** ($\Delta\delta > 400$) could also be due to counterion effects in the experiments. In this context it is interesting to note that quite different values for $\delta(^{55}\mathrm{Mn})$ of **2** have appeared in the literature. In the first study, $\delta = -935$ was given (solvent acetone, counterion not specified) [38]. This value has subsequently been questioned, and $\delta \approx -2000 \pm 200$ has been estimated on the basis of an extrapolation of other literature data [39] (note the good agreement of the mPW1PW91 and B3LYP values in Table 2 with this estimate). The measured value of $\delta = -1{,}445$ was obtained for $[Mn(CO)_6]Cl{\cdot}HCl$ (**12**) in CH_2Cl_2 [11].

In order to model the closely related, neutral $[Mn(CO)_6]Cl$ (**13**), a Cl^- counterion was placed on the threefold axis of **2**, with C_{3v} symmetry imposed. In the optimized structure **13a**, three loose Cl–C contacts are formed and three of the Mn–C distances are significantly elongated (Fig. 3). Two imaginary frequencies at the BP86/AE1 level indicate the presence of minima with lower symmetry. An edge-bridging C_{2v} structure (**13b**) was subsequently found to possess one imaginary frequency. Finally, the minimum was located in the form of C_s symmetric $Mn(CO)_5(COCl)$ (**13c**, Fig. 3). **13b** is the transition structure for the transfer of the Cl atom in **13c**

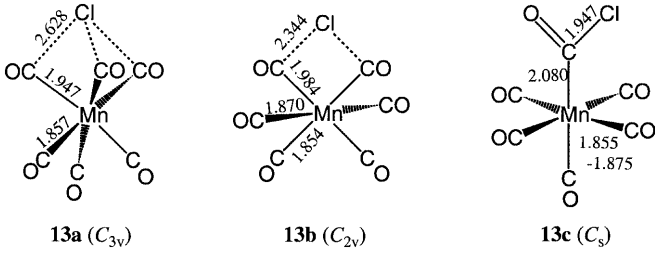

13a (C_{3v}) **13b** (C_{2v}) **13c** (C_s)

Fig. 3. BP86/AE1 optimized stationary points for $[Mn(CO)_6]Cl$ (**13**) including key bond lengths in angstroms

from one carbonyl moiety to another. The barrier for this process is quite low on the potential-energy surface, about 5 kcal/mol, and is further reduced upon inclusion of zero-point, enthalpic, and entropic corrections (Table 3).

On the NMR time scale, **13** should thus display apparent O_h symmetry owing to rapid chlorine exchange between all the carbonyl moieties. Rotation about the Mn–COCl bond in **13c** (required for scrambling of the Cl atom over all six carbonyl moieties) is likely to be rapid, if not essentially free. For the related COMe derivative **6**, the rotational barrier about the Mn–COMe bond is 0.7 kcal/mol at the BP86/AE1 + ZPE level. Interestingly, the computed ^{55}Mn chemical shift of **13c**, $\delta = -1{,}666$ (B3LYP, Table 3), fits better to the experimental value for **12**, $\delta = -1{,}445$, than that of free **2**, $\delta = -1{,}848$ (B3LYP, Table 2). Compound **12** has been described as not very stable, readily decomposing to **4** and other products [40]. While the IR spectrum of **12** in the solid supports the presence of octahedral **2**, an unusually low molar conductivity has been observed [40]. It is quite possible that in solutions of **12**, neutral adducts similar to **13a–c** are populated, which would result in substantial deshielding of the ^{55}Mn resonance with respect to that of free **2**. Further theoretical and experimental work is needed to clarify the nature of the species giving rise to the observed NMR spectra of **12**.

The Cp derivatives **9–11** are prototypical examples for the noncorrelation between oxidation state (or charge) and chemical shift of a transition metal [41]. Even though they are formally Mn(I) d^6 systems, their $\delta(^{55}\text{Mn})$ values cover all but the total chemical shift range of this nucleus (Table 2). It is now well accepted that the chemical shifts for this type of systems are governed by the 3*d* contributions to the paramagnetic part of the shielding tensor, σ^P, which arise from *d–d* excitations centered on the metal [42]. The corresponding key molecular orbitals (MOs) are sketched in Fig. 4 for **10** and **11**. In this orientation, the magnetic operator in the *z* direction cannot couple any of the occupied *d*(Mn) MOs with unoccupied ones. Hence, no strong paramagnetic contributions are expected in that direction, and the corresponding principal component of the chemical shift tensor is the most shielded one, δ_{33} (Fig. 4). For simiar pictorial rationalizations of paramagnetic contributions see, for instance, Refs. [8, 42, 43]. On going from **10** to **11**, the energies of the occupied *d*(Mn) MOs are little affected, while those of the virtual orbitals are significantly lowered. It is the resulting decrease in the energetic separation between magnetically coupled occupied and unoccupied MOs that is responsible for the observed (and computed) deshielding of the ^{55}Mn nucleus. A similar MO scheme is obtained for **9** (not shown), with reduced *d*(Mn) character of the corresponding MOs and even larger energetic separations, consistent with the strongly shielded metal compared to that in **10** and **11**.

Table 3. Computed relative energies (kcal/mol) and ^{55}Mn chemical shifts of the stationary points **13a–c** depicted in Fig. 3

Property/level	**13a**	**13b**	**13c**
E_{rel}/BP86/AE1	7.6	4.9	0.0
(NImag)[a]	(2)	(1)	(0)
E_{rel}/B3LYP/II′[b]	5.4	5.1	0.0
E_{rel}/B3LYP/II′ + ZPE[b,c]	4.6	4.6	0.0
$\Delta H(298)_{rel}$/B3LYP/II′[b,c]	3.9	4.3	0.0
$\Delta G(298)_{rel}$/B3LYP/II′[b,c]	0.9	3.5	0.0
$\delta(^{55}\text{Mn})$/GIAO-B3LYP/II′	−1,018	−1,140	−1,666

[a] Number of imaginary frequencies
[b] Single-point energies for BP86/AE1 geometries
[c] Zero-point, enthalpic, and entropic corrections from the unscaled BP86/AE1 harmonic frequencies

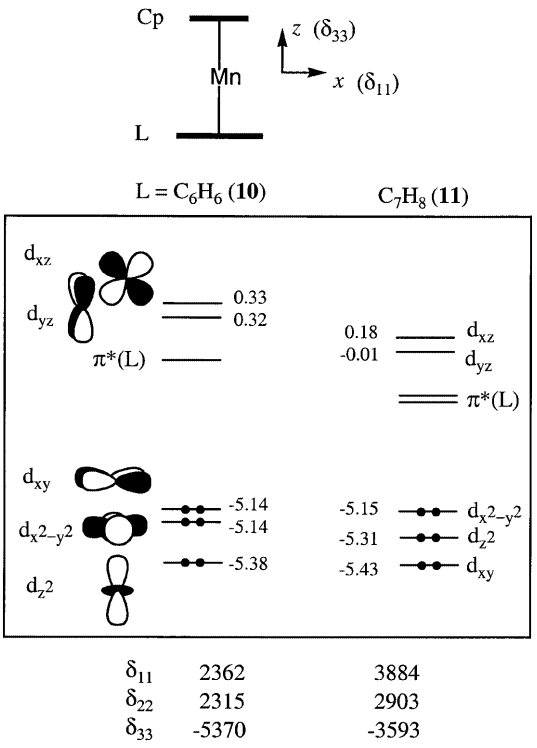

Fig. 4. molecular orbital scheme (*box*) of **10** and **11** including B3LYP/II′ eigenvalues (electron volts) of *d*(Mn)-based molecular orbitals, together with principal components of the chemical shift tensor (*bottom*) and the orientation of the principal axis system (*top*)

3.3 Electric field gradients

Excessive line broadening due to efficient quadrupolar relaxation is one of the main obstacles in transition-metal NMR spectroscopy. When relaxation is dominated by this mechanism, the line width, $\Delta\nu_{1/2}$, should be [44]

$$\Delta\nu_{1/2} \propto q_{zz}^2(1 + \eta^2/3)\tau_c, \quad (1)$$

i.e., it should depend on the largest EFG component q_{zz}, on the asymmetry parameter η defined as $(q_{xx} - q_{yy})/q_{zz}$, and on the molecular correlation time τ_c, which measures the orientational mobility of a molecule and usually increases with molecular size. The asymmetry parameters η enters Eq. (1) via the factor $(1 + \eta^2/3)$, which can only assume values between 1 and 4/3 and is therefore not expected to govern the general trends

observed. In several cases, characteristic variations in transition-metal NMR line widths were observed and rationalized in terms of measured τ_c values and computed EFGs [6, 16].

Even though the EFG, in contrast to the chemical shift, is a simple expectation value and a typical ground-state property, accurate calculations require the use of large basis sets and inclusion of electron correlation at fairly sophisticated levels [45, 46]. On the other hand, trends within a given set of compounds can often be well reproduced qualitatively at lower or intermediate levels, such as Hartree–Fock [16] or DFT [6, 46]. For EFGs of some lighter nuclei, DFT actually performs very well [47], whereas transition-metal nuclei appear to be more challenging (for assessments and applications of computed ^{57}Fe Mößbauer parameters see Ref. [48]). For consistency with the chemical shift calculations discussed previously, EFGs were computed by employing the B3LYP functional, affording the results summarized in Table 4. Values for η are not given, as they are either zero by symmetry or very small (up to 0.05), except for **6** ($\eta = 0.65$).

It follows from Eq. (1) that, if all other factors are equal, there should be a correlation between $\Delta\nu_{1/2}$ and q_{zz}^2. In addition to the corresponding experimental line widths and squares of the computed EFGs, the relative data with respect to the smallest value, obtained for **3**, are given in Table 4, cf. $\Delta\nu_{1/2}$(rel) and q_{zz}^2(rel) entries (in parentheses). There is indeed a noticeable, qualitative correlation between both data sets, spanning roughly two orders of magnitude, which is also apparent in the graphical display in Fig. 5. Thus, the very broad resonances found for **7** and **9**, of the order of 10 kHz, can be traced back to large EFGs, slightly below 1 au. Likewise, the observation that hydride **4** has a much broader signal than the chloro derivative **5** can be explained by the much larger EFG of the former compared to the latter. Apparently, the effect of the EFG on the line widths outweighs that of the correlation time, which, for instance, would serve to sharpen the signal of **4** relative to that of **5**.

As already noted, the computed q_{zz} values of the metal are not expected to be of quantitative accuracy

Table 4. B3LYP/II′ computed electric field gradients (largest components q_{zz} of the electric field gradient tensor) of the Mn nucleus in organomanganese complexes, together with experimental line widths [Experimental data (Hz), from Refs. [10, 11, 12], except for **8** (B. Wrackmeyer, personal communication). In *parentheses*: values relative to **3**

Molecule	q_{zz}	q_{zz}^2 (rel)[a]	$\Delta\nu_{1/2}$	(rel)[a]
$Mn_2(CO)_{10}$ (**3**)	0.076	(1)	83	(1)
$Mn(CO)_5Cl$ (**5**)	0.081	(1.1)	331	(4.0)
$Mn(NO)_3(CO)$ (**8**)	0.002	(0.001)	1,270	(15.3)
$Mn(Cp)(C_6H_6)$ (**10**)	0.602	(62.7)	1,500	(18.1)
$Mn(Cp)(C_7H_8)$ (**11**)	0.661	(79.1)	2,250	(27.1)
$Mn(CO)_5H$ (**4**)	0.646	(72.3)	4,147	(50.0)
$Mn(CO)_5COMe$ (**6**)	0.367	(23.3)	4,300	(51.8)
$Mn(Cp)(CO)_3$ (**9**)	0.948	(155.6)	10,039	(121.0)
$Mn(CO)_5^-$ (**7**)	0.919	(146.2)	10,585	(127.5)

[a] Relative to **3**

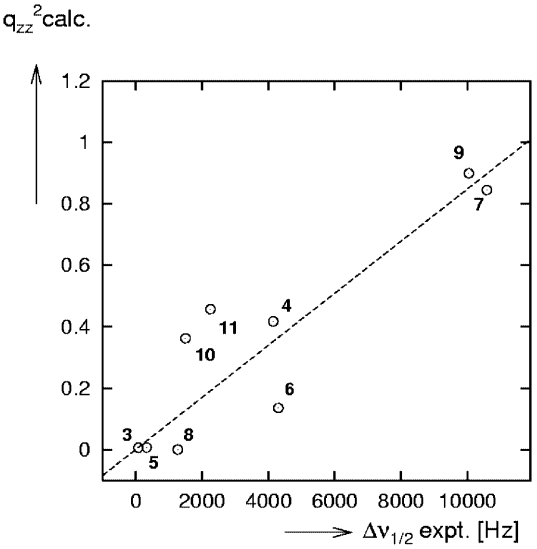

Fig. 5. Computed electric field gradient contributions to $\Delta\nu_{1/2}$ (B3LYP/II′ level for BP86/AE1 geometries) versus the actual, observed line widths. A linear regression line through the origin is shown to guide the eye

and include errors due to the density functional and incomplete basis sets employed, as well as from neglect of rovibrational and solvent effects. In Ref. [6] ^{99}Ru EFGs, computed at a comparable level as in the present study, were found to be systematically overestimated (up to about 60%) with respect to Mößbauer-derived data. Even with exactly computed EFGs, one should bear in mind that no perfect correlation between $\Delta\nu_{1/2}$(rel) and q_{zz}^2(rel) can be expected, because the experimental $\Delta\nu_{1/2}$ data contain, in addition, the dependence on τ_c. The latter is affected by molecular size, viscosity of the solvent, concentration, and temperature. Of these parameters at least the first two usually vary from one experiment to the other. In view of these limitations, the qualitative agreement between the $\Delta\nu_{1/2}$(rel) and q_{zz}^2(rel) values in Table 4 is quite remarkable. Theoretical EFGs are thus a straightforward way to quantify the "asymmetry of the electron distribution" around the metal nucleus, and could be used to predict if the ^{55}Mn signal of a given compound can be detected or not. On the basis of the data in Table 4, it would seem very difficult to record the ^{55}Mn spectrum of a compound with q_{zz} significantly larger than 1 au.

4 Conclusions

An assessment of GGA and hybrid DFT levels for the computation of ^{55}Mn NMR properties has been presented for a representative set of organometallic Mn compounds. For the description of chemical shifts, hybrid functionals, in particular the popular B3LYP combination, have been found to be superior to the pure BPW91 functional. The same had previously been found for all other transition metals studied so far, with the sole exception of ^{95}Mo. Mean absolute errors with respect to experiment are somewhat larger for $\delta(^{55}$Mn)

than those attainable for the other metals with the same methods. In one case, $Mn(CO)_6^+$, part of this discrepancy may be due to effects on the Mn shielding exerted by the counterions present in the experiments.

Trends in EFGs computed at the B3LYP/II′ level roughly parallel those in the observed ^{55}Mn NMR line widths, consistent with the dominant quadrupolar relaxation mechanism expected for this nucleus. As EFGs are fairly easy to calculate, at least in a qualitative manner, the computation of this property can be useful to predict if the ^{55}Mn NMR signal of a given, new compound can be detected.

In summary, the DFT levels necessary for the theoretical treatment of ^{55}Mn chemical shifts and, more qualitatively, line widths have been identified, allowing the prediction and interpretation of ^{55}Mn NMR parameters. Such computations can be a valuable complement to ^{55}Mn NMR spectroscopy, a useful and versatile analytical tool for Mn compounds.

Acknowledgements. The author thanks W. Thiel for his continuous support, the Deutsche Forschungsgemeinschaft for a Heisenberg fellowship, and B. Wrackmeyer for communicating an unpublished result. The calculations were carried out on a Medion 1.8 GHz personal computer.

References

1. Koch W, Holthausen MC (2000) A chemist's guide to density functional theory. Wiley-VCH, Weinheim, and references therein
2. Davidson ER (2000) Chem Rev 100: 351
3. (a) Bühl M, Kaupp M, Malkin VG, Malkina, OL (1999) J Comput Chem 20: 91; (b) Schreckenbach G, Ziegler T (1998) Theor Chem Acc 99: 71
4. Bühl M (1997) Chem Phys Lett 267: 251
5. Bühl M, Hamprecht FA (1998) J Comput Chem 119: 113
6. Bühl M, Gaemers S, Elsevier CJ (2000) Chem Eur J 6: 3272
7. Godbout N, Oldfield E (1997) J Am Chem Soc 119: 8065
8. Bühl M (1999) Eur J Chem 5: 3514
9. Wilson PJ, Amos RD, Handy NC (2000) Phys Chem Chem Phys 2: 187
10. Pregosin PS (1991) In: Pregosin PS (ed) Transition metal nuclear magnetic resonance. Elsevier, Amsterdam, pp 90–101
11. Keçeci A, Rehder D (1981) Z Naturforsch 36b: 20
12. (a) Torocheshnikov V, Rentsch D, von Philipsborn W (1994) Magn Reson Chem 32: 348; (b) Wrackmeyer B, Hofmann T, Herberhold M (1995) J Organomet Chem 486: 255
13. (a) Gaemers S, van Slageren J, O'Connor CM, Vos JG, Hage R, Elsevier CJ (1999) Organometallics 18: 5238–5244; (b) Wrackmeyer B, Ayazi A, Maisel HE, Herberhold M (2001) J Organomet Chem 630: 263; (c) Janiak C, Dorn T, Paulsen H, Wrackmeyer B (2001) Z Anorg Allg Chem 627: 1668
14. von Philipsborn W (1999) Chem Soc Rev 28: 95
15. Pregosin PS (ed) (1991) Transition metal nuclear magnetic resonance. Elsevier, Amsterdam
16. (a) Bühl M, Hopp G, von Philipsborn W, Beck S, Prosenc M, Rief U, Brintzinger HH (1996) Organometallics 15: 778; (b) Bühl M (1996) Magn Reson Chem 34: 782
17. Becke AD (1988) Phys Rev A 38: 3098
18. (a) Perdew JP (1986) Phys Rev B 33: 8822; (b) Perdew JP (1986) Phys Rev B 34: 7406
19. (a) Wachters AJH (1970) J Chem Phys 52: 1033; (b) Hay PJ (1977) J Chem Phys 66: 4377
20. (a) Hehre WJ, Ditchfield R, Pople JA (1972) J Chem Phys 56: 2257; (b) Hariharan PC, Pople JA (1973) Theor Chim Acta 28: 213
21. Cheeseman JR, Trucks GW, Keith TA, Frisch MJ (1996) J Chem Phys 104: 5497
22. (a) Perdew JP (1991) In: Ziesche P, Eischrig H (eds) Electronic structure of solids. Akademie, Berlin, pp; (b) Perdew JP; Wang Y (1992) Phys Rev B 45: 13244
23. Adamo C, Barone V (1998) J Chem Phys 108: 664
24. Becke AD (1993) J Chem Phys 98: 5648
25. Lee C, Yang W, Parr RG (1988) Phys Rev B 37: 785
26. Kutzelnigg W, Fleischer U, Schindler M (1990) In: NMR basic principles and progress, vol 23. Springer, Berlin Heidelberg New York, pp 165–262
27. Frisch MJ, Trucks GW, Schlegel HB, Scuseria GE, Robb MA, Cheeseman JR, Zakrzewski VG, Montgomery JA Jr, Stratmann RE, Burant JC, Dapprich S, Millam JM, Daniels AD, Kudin KN, Strain MC, Farkas O, Tomasi J, Barone V, Cossi M, Cammi R, Mennucci B, Pomelli C, Adamo C, Clifford S, Ochterski J, Petersson GA, Ayala PY, Cui Q, Morokuma K, Salvador P, Dannenberg JJ, Malick DK, Rabuck AD, Raghavachari K, Foresman JB, Cioslowski J, Ortiz JV, Baboul AG, Stefanov BB, Liu G, Liashenko A, Piskorz P, Komaromi I, Gomperts R, Martin RL, Fox DJ, Keith T, Al-Laham MA, Peng CY, Nanayakkara A, Challacombe M, Gill PMW, Johnson B, Chen W, Wong MW, Andres JL, Gonzalez C, Head-Gordon M, Replogle ES, Pople JA (2001) Gaussian 98, revision A.11. Gaussian, Pittsburgh, PA
28. Palenik JG (1967) Inorg Chem 6: 503
29. Bianchi R, Gervasio G, Marabello D (2000) Inorg Chem 39: 2360
30. La Placa SJ, Hamilton WC, Ibers JA, Davison A (1969) Inorg Chem 8: 1928
31. Greene PT, Bryan RF (1971) J Chem Soc A 1559
32. Frenz BA, Ibers JA (1972) Inorg Chem 11: 1109
33. Cowie J, Hamilton EJM, Laurie JCV, Welch AJ (1990) J Organomet Chem 394: 1
34. Herberhold M, Hofmann T, Milius W, Wrackmeyer B (1994) J Organomet Chem. 472: 175
35. Almenningen A, Jacobsen GG, Seip HM (1969) Acta Chem Scand 23: 685
36. Robiette AG, Sheldrick GM, Simpson RNF (1969) J Mol Struct 4: 221
37. (a) Malkin VG, Malkina OL, Steinebrunner G, Huber H (1996) Chem Eur J 2: 452; (b) Pfrommer BG, Mauri F, Louie SG (2000) J Am Chem Soc 122: 123; (c) Bühl M, Parrinello M (2001) Chem Eur J 7: 4487; (d) Bühl M, Mauschick FT, Terstegen F, Wrackmeyer B, Angew Chem (in press)
38. Nakano T (1977) Bull Chem Soc Jpn 50: 661
39. Kidd RG (1980) Annu Rep NMR Spectrosc 10A: 1
40. Kruck T, Noack M (1964) Chem Ber 97: 1693
41. Wrackmeyer B (1994) Chem Unser Zeit 28: 309
42. Kanda K, Nakatsuji, H, Yonezawa T (1984) J Am Chem Soc 106: 5888
43. Ruiz-Morales Y, Ziegler T (1998) J Phys Chem A 102: 3970
44. Abragam A (ed) (1961) The principles of nuclear magnetism. Oxford University Press, Oxford, p 314
45. (a) Hemmingsen L, Ryde U (1996) J Phys Chem 100: 4803; (b) Kellö V, Sadlej A, Pyykkö P, Sundholm D, Tokman M (1999) Chem Phys Lett 304: 414
46. Gee M, Wasylishen RE (1999) In: Facelli JC, de Dios AD (eds), Modeling NMR chemical shifts. ACS symposium series 732. American Chemical Society, Washington, DC, p 259
47. (a) Fedotov MA, Malkina OL, Malkin VG (1996) Chem Phys Lett 258: 330; (b) Bailey WC (2000) Chem Phys 252: 57
48. (a) Schwerdtfeger P, Söhnel T, Pernpointer M, Laerdahl JK, Wagner FE (2001) J Chem Phys 115: 5913; (b) Havlin RV, Godbout N, Salzmann R, Wojdelski M, Arnold W, Schulz CE, Oldfield E (1998) J Am Chem Soc 120: 3144